Acta Geochim (2018) 37(2):310–322
https://doi.org/10.1007/s11631-017-0216-9

ORIGINAL ARTICLE

The use of in-situ cosmogenic ^{21}Ne in studies on long-term landscape development

Yan Ma[1,2] · **Finlay M. Stuart**[2]

Received: 15 February 2017 / Revised: 21 April 2017 / Accepted: 16 August 2017 / Published online: 28 August 2017

Abstract Cosmogenic Ne isotopes are stable and are routinely used for constraining the timing of events and the rate of surface change beyond the limit that can be studied with radionuclides ^{10}Be, ^{26}Al, and ^{36}Cl. Cosmogenic Ne analysis can be used in quartz and in a range of other minerals. Analysis typically requires significantly less material than do cosmogenic ^{10}Be and ^{26}Al, opening up the technique for small samples—individual pebbles in river sediments, for example. Analysis is easier and faster than for radionuclides, not least because Ne measurements do not require significant chemical procedures. However, the presence of other sources of Ne in minerals tends to restrict the use of cosmogenic ^{21}Ne to old landscapes and long exposure durations. In this review we briefly outline the background of cosmogenic Ne production in rocks and minerals at the Earth's surface, then document the key uses of the technique by highlighting some earlier studies, and finish with a short perspective on the future of the technique.

Keywords Cosmogenic nuclides · ^{21}Ne · Long timescale · Landscape evolution

✉ Yan Ma
mayan82634@hotmail.com

[1] State Key Laboratory of Earthquake Dynamics, Institute of Geology, China Earthquake Administration, Beijing 100029, China

[2] Isotope Geosciences Unit, Scottish Universities Environmental Research Centre, Scottish Enterprise Technology Park, East Kilbride G75 0QF, UK

1 Introduction

The last two decades have seen the development of routine techniques for determining the concentration of cosmogenic nuclides in terrestrial rocks and minerals. The widespread application of, in particular, cosmogenic radionuclides has led to a steep change in knowledge of the timing and rates of Earth surface processes (Gosse and Phillips 2001). The headline applications of the technique have included the precise determination of deglaciation timescales (e.g., Ivy-Ochs et al. 2006), the slip history of faults (e.g., Benedetti et al. 2002), the erosion rate of river catchments (e.g., Portenga and Bierman 2011), and the time of sediment burial in order to determine rates of landscape evolution (e.g., Granger and Riebe 2007).

The vast majority of terrestrial cosmogenic nuclide studies have exploited the radioactive nuclide ^{10}Be in quartz. Stable cosmogenic nuclides ^{3}He and ^{21}Ne have higher production rates than the radionuclides, and can be measured on conventional gas source mass spectrometers that are significantly less expensive and require less manpower to operate than the accelerator mass spectrometers (AMS) required for radionuclides. Despite this relative efficiency, cosmogenic nuclides have been exploited far less routinely. This is due in large part to the presence of other sources of ^{3}He and ^{21}Ne in minerals that must be quantified precisely prior to successful application of the technique. Diffusive loss of cosmogenic ^{3}He from quartz limits the technique to mafic minerals such as olivine, pyroxene, and FeO (e.g., Foeken et al. 2009; Margerison et al. 2005). Despite this restriction it has a broad range of applications, from constraining the evolution of Cenozoic ice history of Antarctica (Kong et al. 2010; Margerison et al. 2005) and the topographic evolution of mountain belts (Evenstar et al. 2015) to determining the timing of the

collapse of volcanic edifices in the Holocene (Foeken et al. 2009). Cosmogenic ^{21}Ne is retained in quartz. In addition to providing a useful complement to cosmogenic radionuclides, ^{21}Ne has proven to be a powerful tracer of long-term landscape change, particularly of slowly eroding landscapes.

In this paper, we first review all aspects of the production of cosmogenic ^{21}Ne in minerals at the Earth's surface, then discuss the techniques that are commonly used for Ne isotope measurement. This is followed by a short explanation of the complications generated by the production of Ne by nuclear reactions in minerals, and trapped air-derived Ne. We finish with an overview of recent advances in the application of cosmogenic ^{21}Ne to long-term landscape development. This last topic is separated into two sections: studies that concentrate on exposure age determinations and those that aim to quantify erosion rates.

2 Background

2.1 Production of terrestrial in-situ cosmogenic isotopes

Terrestrial in-situ produced cosmogenic nuclides are generated by interactions of secondary cosmic-ray particles with target nuclei in minerals near the Earth's surface. There are three main nuclide production pathways: (1) spallation reaction by fast and high-energy secondary cosmic ray particles, where neutrons are the dominant particle. The intensity of neutrons is attenuated exponentially in the rock due to nuclear interactions and ionization losses (Lal and Peters 1967). The attenuation of energy and flux of the cosmic-ray particles provides the possibility for the studies of surficial processes with in-situ produced cosmogenic nuclides, whose production rates beneath rock surfaces are dependent on the intensity of neutrons and can be modeled by an exponential function of depth in the surface material (Lal 1991). (2) negative muon capture and (3) fast muon-induced reactions. Negative muon-induced production is only significant at a depth of 2.5–3 m in most rocks, where the high-energy neutron flux is less than 1% of the surface. Fast muons have sufficiently high energy to cause neutron reactions, but due to their very low abundance they only become important at great depth where no other secondary cosmic-ray particles survive. Muon-induced reactions contribute only a few percent to the total cosmogenic nuclide production in surface rocks of the Earth (e.g., Borchers et al. 2016; Braucher et al. 2011; Marrero et al. 2016).

Due to atmospheric and geomagnetic shielding, the cosmic ray particle flux, and therefore cosmogenic nuclide production rates at the Earth's surface, vary with altitude and geomagnetic latitude. Consequently, the rate of nuclide production must be scaled with the variation of latitude and elevation. Scaling is mainly based on measurements of the present day cosmic ray flux. The first model was based on photographic records of spallation events in photo-emulsions (Lal 1991). This model was subsequently modified to account for the effect of pressure (Balco et al. 2008; Stone and Vasconcelos 2000). The majority of scaling models are based on the global neutron monitor network that is maintained by the cosmic-ray physics community (Desilets and Zreda 2003; Desilets et al. 2006; Dunai 2001; Lifton et al. 2005). These models scale production with altitude in regions of high magnetic strength. Most recently, Lifton et al. (2014) used numerical simulations of cosmic-ray modulation by the geomagnetic field and the atmosphere, calibrated against atmospheric differential flux measurements for neutrons and protons. Collectively these models produced small differences in cosmogenic nuclide production rates. Production rates are typically normalized to sea level high latitude (SLHL).

The measurement of absolute production rates of commonly-used cosmogenic nuclides generally uses natural calibration sites, with the accumulated cosmogenic nuclide concentration measured in a rock surface of known age (e.g., Balco and Shuster 2009b). These calibration sites must be old enough to have accumulated measurable nuclide concentrations, but young enough to have avoided significant degradation by weathering and erosion. Phillips et al. (2016) reviewed the prevailing radionuclide calibration studies and introduced cosmogenic ^{10}Be, ^{26}Al, and ^{36}Cl data for four new calibration sites that were selected by the CRONUS-Earth project. Goehring et al. (2010) reviewed the prevailing calibration sites for ^{3}He production rate, though work is ongoing (Foeken et al. 2012).

2.2 Cosmogenic neon

Neon has three stable isotopes, ^{20}Ne, ^{21}Ne, and ^{22}Ne, of which ^{20}Ne is the most abundant in the atmosphere (90.50%). All three neon isotopes are produced at similar rates by cosmic ray secondary neutron spallation reactions in rocks. Due to their lower natural abundance in air, ^{21}Ne and ^{22}Ne concentrations are more sensitive to cosmogenic production in minerals. Cosmogenic ^{21}Ne is generally adopted as the parameter that reflects the surface exposure history as its production rate is high in comparison to the amount present in minerals.

Cosmogenic Ne isotopes are produced largely from the target elements Na, Mg, Al, and Si, as these have the largest reaction cross-sections and are closest in mass to Ne. Cosmogenic Ne is quantitatively retained by most silicates (Shuster and Farley 2005). The ubiquity of quartz at the

Earth surface means it is the dominant target mineral, but olivine and pyroxene are used in studies of igneous rocks.

Atmosphere-derived Ne is ubiquitous in minerals. At its simplest, the Ne isotope composition of surface-exposed minerals reflects the two-component mixture of atmospheric and cosmogenic neon. This mixing line is defined by the "spallation line" in the Ne three-isotope diagram (Fig. 1). The slope of the spallation line depends on mineral composition; cosmogenic $^{21}Ne/^{22}Ne$ values determined experimentally for quartz are 1.120 ± 0.020 (Niedermann et al. 1993) and 1.143 ± 0.038 (Schäfer et al. 1999). The corresponding value for pyroxene is similar, 1.055 ± 0.017 (Bruno et al. 1997).

Determining the production rate of cosmogenic ^{21}Ne is more difficult than for the radionuclides and ^{3}He, due to a relatively low production rate compared to atmospheric concentration in minerals. The first determination of cosmogenic ^{21}Ne production rates in quartz was reported by Niedermann et al. (1994). Based on the production rate ratio of $^{21}Ne/^{26}Al$ (0.65 ± 0.11)—which was considered to be equal to the nuclide concentration ratio in short-exposed quartz samples [having an assumed age of 11 ka based on radiocarbon dates from Nishiizumi et al. (1989)] collected from a glacially polished granite surface in the Sierra Nevada, California, USA—the cosmogenic ^{21}Ne production rate was determined to be 21 atoms·g^{-1}·a^{-1}. These authors managed to distinguish the various neon components contained in the Sierra Nevada rock samples by isotopic signatures and release systematics. They measured all three neon isotopes in stepwise gas extraction to evaluate the cosmogenic neon and trapped components, including both atmospheric and inherited components. Nucleogenic neon impacted the precision of the measurement of the extremely low concentration of cosmogenic neon in this short-exposed quartz. Nevertheless, the authors showed a $^{21}Ne/^{26}Al$ ratio with an uncertainty of 17%. Niedermann (2000) revised the rate to 19.0 ± 3.7 atoms·g^{-1}·a^{-1} after adopting a revised exposure age of 13 ka (Clark et al. 1995), and used the geomagnetic latitude of the sampling site to scale the production rate to SLHL.

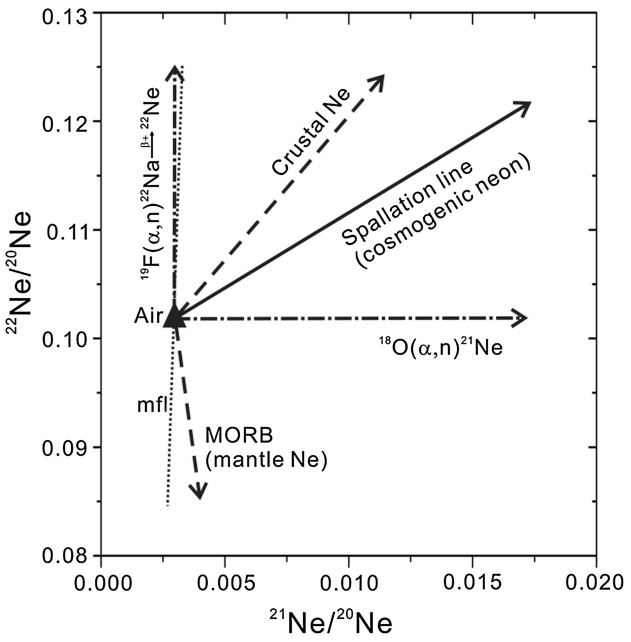

Fig. 1 Neon three-isotope diagram ($^{22}Ne/^{20}Ne$ vs. $^{21}Ne/^{20}Ne$) showing the compositions and trends of various Ne components (Niedermann 2002). *mfl* mass fractionation line

According to the latest report about cosmogenic nuclide production rate calibration (Phillips et al. 2016), the SLHL production rate of ^{10}Be, which is converted from the primary calibration site production rate using the Lal-Stone scaling method, is 4.01 atoms g^{-1}·a^{-1}. Based on this updated ^{10}Be production rate, the cosmogenic ^{21}Ne production rate (SLHL) has been revised to 15.69 atoms g^{-1}·a^{-1}.

Balco and Shuster (2009b) reported an independent determination of ^{21}Ne production rate in quartz. Instead of relying on a single calibration site with short exposure history, they selected sites in the Antarctic Dry Valleys where the surface ^{21}Ne concentration has reached steady state between nuclide production and loss by surface erosion. Relatively high cosmogenic nuclide concentrations allow the high accuracy of nuclide concentration ratio determination. Combining the steady-state surface concentration ratio of $^{21}Ne/^{10}Be$ with the then-established ^{10}Be production rate of 4.61 atoms·g^{-1}·a^{-1}, they determined the total ^{21}Ne production rate to be 18.3 ± 0.4 atoms·g^{-1}·a^{-1} (SLHL) in quartz. Using the new ^{10}Be production rate (Phillips et al. 2016), the cosmogenic ^{21}Ne production rate (SLHL) is 15.9 atoms·g^{-1}·a^{-1} in quartz.

In the same year, Goethals et al. (2009a) used quartz collected from the surface of the Bishop Tuff in eastern California with an $^{40}Ar/^{39}Ar$ age of 760 ± 2 ka (Van den Bogaard and Schirnick 1995) to determine the cosmogenic ^{21}Ne production rate. The precise exposure age of the tuff and its relatively high cosmogenic nuclide concentrations are crucial for the accuracy of nuclide production rate determination. The authors first measured concentrations of cosmogenic ^{10}Be and ^{21}Ne; then, based on the conservative estimate of the surface erosion rate using the tuff $^{40}Ar/^{39}Ar$ age and their previously published ^{21}Ne concentrations, they determined the $^{10}Be/^{21}Ne$ production rate ratio assuming steady-state erosion. When combined with the production rate of ^{10}Be of 4.61 atoms·g^{-1}·a^{-1}, the production rate ratio converted to a quartz ^{21}Ne SLHL production rate of 19.9 atoms·g^{-1}·a^{-1}. Again, using the new ^{10}Be production rate (Phillips et al. 2016), the ^{21}Ne production rate (SLHL) is 17.3 atoms·g^{-1}·a^{-1}.

2.3 Calculation of exposure ages and surface erosion rates

For stable cosmogenic nuclides, age determinations assume that the concentration of cosmogenic ^{21}Ne, $N(z, t)$, accumulates in surface materials with exposure age, t. At any subsurface depth z, the temporal evolution of $N(z, t)$ in the rock can be expressed as (Lal 1991):

$$\frac{\mathrm{d}N(z,t)}{\mathrm{d}t} = P(z,t). \quad (1)$$

where $P(z, t)$ is the production rate of the cosmogenic nuclide at the depth below the rock surface, and the temporal variation of production rate due to solar activity or geomagnetic field changes is assumed to be negligible, i.e., $P(z, t) = P(z)$. Assuming the rates of nuclide production induced by both spallation and muon reactions decrease exponentially with depth,

$$P(z) = P_{\mathrm{n}}(z) + P_{\mu}(z) = P_{\mathrm{n}}(0) \cdot \mathrm{e}^{-\rho z/\Lambda_{\mathrm{n}}} + P_{\mu}(0) \cdot \mathrm{e}^{-\rho z/\Lambda_{\mu}} \quad (2)$$

where $P_{\mathrm{n}}(0)$ and $P_{\mu}(0)$ are the rates of nuclide production induced by spallation reaction and muon reaction, respectively, at the rock surface; ρ is the rock density; and Λ_{n} and Λ_{μ} are the attenuation length (g·cm^{-2}) of the particles causing the spallation reaction and muon reaction, respectively. The value of Λ_{n} is determined by experiment and calculation, with the widely used value ranging from 157 to 167 g·cm^{-2} (Masarik and Reedy 1995). The value of Λ_{μ} can be approximated as around 1300 g·cm^{-2} (Barbouti and Rastin 1983; Brown et al. 1995), or can use more accurate mathematical representations, including the interactions with both stopped and fast muons, reported by Granger and Smith (2000).

For eroding landforms, z is time dependent, and $z(t)$ can be defined using erosion rate on the surface, $\varepsilon(t)$, according to the following equation (Lal 1991; Niedermann 2002):

$$z(t) = \int_0^t \varepsilon(t) \cdot dt + const. \quad (3)$$

Defining the initial shielding depth z_0 at time of $t = 0$, and considering a case of constant erosion rate, i.e. $\varepsilon(t) = \varepsilon$, the depth at time t is $z(t) = z_0 - \varepsilon \cdot t$.

Then for the differential Eq. (1), we can obtain the solution for stable nuclide concentration at the rock surface, $N(t)$ (Niedermann 2002):

$$N(t) = N(0) + \frac{P_{\mathrm{n}}(0)}{\rho\varepsilon/\Lambda_{\mathrm{n}}} \cdot (1 - \mathrm{e}^{-\rho\varepsilon \cdot t/\Lambda_{\mathrm{n}}}) + \frac{P_{\mu}(0)}{\rho\varepsilon/\Lambda_{\mu}} \cdot (1 - \mathrm{e}^{-\rho\varepsilon \cdot t/\Lambda_{\mu}}) \quad (4)$$

where $N(0)$ is the initial nuclide concentration in the rock at the moment $t = 0$ inherited from all previous exposure events.

Equation (4) illustrates the relationship of cosmogenic ^{21}Ne concentration with both exposure duration and erosion rate, but gives only the minimum exposure age and the maximum erosion rate from a measured cosmogenic nuclide concentration in a sample. The measurement of two cosmogenic nuclides with different half-lives in the same sample can be used to constrain exposure age and erosion rate. ^{21}Ne is commonly coupled with ^{10}Be as both can be measured in the same quartz sample to investigate the history of old surfaces. The temporal evolution of the nuclide concentration ratio ^{21}Ne/^{10}Be for various erosion rates is plotted in Fig. 2, in which the area between the two curves, steady-state erosion island (Lal 1991), comprises all possible combinations of steady-state erosion and simple exposure histories (Lal 1991; Niedermann 2002). However, complex exposure, e.g., periods of burial, will also change the ratio of the two nuclides due to ^{10}Be decay (Fig. 2). In the case that a surface experienced exposure, was buried for a period and re-exposed, the concentrations of the radionuclides ^{10}Be and ^{26}Al will return to equilibrium with steady erosion if the re-exposure time is long enough, so ^{10}Be/^{26}Al will not reflect the complex exposure history. When adding ^{21}Ne measurements to ^{10}Be or ^{26}Al, ^{21}Ne concentration—which is totally preserved and

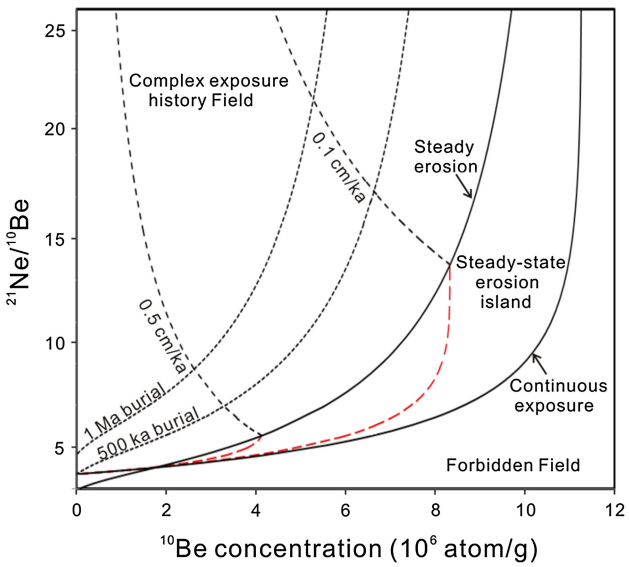

Fig. 2 Plot of the concentration ratio ^{21}Ne/^{10}Be versus the ^{10}Be concentration, generated using CosmoCalc version 1.7 (Vermeesch 2007) using the production rate of 5.16 atoms·g^{-1}·a^{-1} for ^{10}Be and 19.3 atoms·g^{-1}·a^{-1} for ^{21}Ne. The *lower solid line* represents the temporal evolution of these two values in the continuous exposed surface without the effect of erosion, the *upper solid line* in steady-state erosion condition. *Dash lines* indicate the temporal evolution under erosion rates of 0.5 and 0.1 cm/ka; *dotted lines* under different burial periods of 1 and 0.5 Ma. The area between the "continuous exposure" curve and the "steady erosion" curve is "steady-state erosion island", which comprise all possible combinations of exposure ages and erosion rates for simple exposure histories

requires a much longer time to reach steady state with a new erosion rate—will retain the information about previous periods of exposure and burial.

3 Measurement of cosmogenic ^{21}Ne

Cosmogenic Ne analysis is generally performed on between 5 mg and 1 g of pure mineral. Typically this is quartz, but olivine and pyroxene have been analyzed fairly routinely. This compares to 5–30 g of quartz that is usually required for ^{10}Be and ^{26}Al determinations by AMS. Sample preparation is largely restricted to the physical extraction of a discrete mineral phase from rock. Separation relies on density methods (e.g. shaker table and heavy liquids) and magnetic techniques. The target mineral-rich fraction is usually inspected under a binocular microscope and contaminating grains are removed by hand. Chemical processing of mineral samples is typically restricted by variations of the Kohl and Nishiizumi (1992) leaching procedure in order to remove the outer few 10's μm of mineral which may have nucleogenic Ne generated by implanted particles and neutrons. Samples are typically ultrasonically cleaned with deionized water to remove traces of HF from mineral surfaces, then with acetone to remove contaminating trace hydrocarbons.

Typical analysis amounts range from 10 to 250 mg of each sample, depending on the Ne concentration. Samples are typically wrapped in metal foil—Al, Pt or Nb—in order to withstand vacuum systems. Gas extraction is typically undertaken either in double-vacuum resistance furnaces (e.g., Codilean et al. 2008) or using near-visible wavelength lasers to heat mineral samples directly (Balco and Shuster 2009b). Samples are usually pumped to ultra-high vacuum levels for many hours, sometimes heating to 50–70 °C prior to analysis, to remove absorbed atmospheric Ne.

Cosmogenic Ne is extracted by heating each sample in one step (typically 1300 °C) or in several temperature steps in order to identify different Ne components. Active gases are removed by exposure to hot metal surfaces, usually ZrAl getter pumps or Ti sublimation pumps. The heavy noble gases and residual active gases are absorbed on liquid nitrogen-cooled traps of either activated charcoal or sintered metal. Getter pumps operated at room temperature are used to absorb hydrogen. Helium is removed by absorbing the residual gases onto cryostatic cold head.

Neon isotope analysis is done in static mode using high-resolution magnetic sector mass spectrometers. These typically employ Nier-type electron impact ion sources tuned to optimize sensitivity for Ne ionization. Ion beam intensities are measured using electron multiplier, usually in peak jumping mode. The mass spectrometers usually contain room temperature getter pumps and a liquid nitrogen-cooled trap in order to minimize the contribution of interfering species during analysis.

On all but the latest high-resolution noble gas mass spectrometers, isobaric interferences at mass 20, 21, and 22 require correction. This entails measurement of the abundances of masses 2, 16, 18, 19, 20, 21, 22, 40, and 44. Instrumental sensitivity and mass fractionation in the instrument are calculated from repeated analysis of aliquots of Ne in air. In many laboratories the CREU quartz standard (Ma et al. 2015; Vermeesch et al. 2015) is used as an internal check.

The abundance of cosmogenic ^{21}Ne ($^{21}Ne_c$) in samples is calculated assuming all measured ^{20}Ne ($^{20}Ne_m$) is atmospheric in origin from:

$$^{21}Ne_c = {}^{21}Ne_m \times \frac{\left[\left(^{21}Ne/^{20}Ne\right)_m - \left(^{21}Ne/^{20}Ne\right)_{air}\right]}{\left(^{21}Ne/^{20}Ne\right)_m} \quad (5)$$

Unresolved contributions to ^{20}Ne occur as a result of $H_2^{18}O^+$, $^{40}Ar^{2+}$, and HF^+. Interference at $m/e = 20$ from $H_2^{18}O^+$ is calculated from the measurement of $H_2^{16}O^+$ at mass 18. The $^{19}F^+$ signal is constant in mass spectrometer background, blank, calibration, and sample measurements indicating that fluorine is dominant in the mass spectrometer. The absence of an effect of $H^{19}F^+$ on blank measurements implies that it is unimportant for measurement of samples' ^{20}Ne. The dominant interference at $m/e = 20$ comes from $^{40}Ar^{2+}$. The charge state ratio $^{40}Ar^+/^{40}Ar^{2+}$ is governed by the partial pressure of H in the mass spectrometer ionization region. A first-order relationship between $^{40}Ar^+/^{40}Ar^{2+}$ and H^+ beam size is recorded in many laboratories. The aim is to ensure that partial pressure of H remains constant throughout the analysis periods. Correction for $^{12}C^{16}O_2{}^{2+}$ at $m/e = 22$ is calculated from measured mass 44 ($^{12}C^{16}O_2{}^+$) using $CO_2{}^{2+}/CO_2{}^+$ determined by repeated measurements interspersed with sample measurements. Correction for $^{63}Cu^{3+}$ at ^{21}Ne can be done by measuring $^{65}Cu^{3+}$.

Although all three isotopes of neon need to be measured when calculating the cosmogenic ^{21}Ne concentration, the uncertainty mainly derives from the measurement error of ^{21}Ne, usually around 5%. In cases of high ^{21}Ne content, the error can go down to ~3%, approaching the lower limit for cosmogenic ^{21}Ne measurement uncertainty. Consequently, measurement uncertainty is commonly larger for ^{21}Ne than for the radionuclides ^{10}Be or ^{26}Al. However, ^{21}Ne is a stable isotope, so it eliminates the uncertainty from the determination of the radionuclide decay constant, which is known to be ~1% for ^{10}Be and ~3% for ^{26}Al (Balco and Shuster 2009a).

As to the precision of the final exposure age or erosion rate, it depends not only on the precision of the parameters involved in data calculation, such as the measured isotope

content, the decay constant of the isotope, the nuclide production rate, and the scaling factor of production rate, but also on the reliability of the model we adopt in the given situation. For example, age uncertainty depends more on whether the assumption of the simple/complex exposure history is appropriate for what the sample has undergone. As a result, the total uncertainty is high in some geological situations if all error sources are considered, both for ^{21}Ne and for radionuclides. However, cosmogenic ^{21}Ne is produced and retained in a range of minerals and thus has the potential to constrain the timing of the exposure of surfaces that cannot be studied with ^{10}Be and ^{26}Al. Furthermore, the unique possibility of stable ^{21}Ne isotope for quantitative geomorphologic studies in the low-erosion region also endows it with huge potential to become a powerful tool which cannot be replaced by radionuclides or other techniques.

4 Neon isotope components in minerals

There are several sources of isotopically-distinct Ne in minerals that must be quantified before the concentration of cosmogenic Ne can be determined.

4.1 Air

Neon is present with a volume concentration of 18.2 ppm in air. It has three stable isotopes—^{20}Ne, ^{21}Ne, and ^{22}Ne—and the atmospheric isotopic ratios of ^{21}Ne/^{20}Ne and ^{22}Ne/^{20}Ne are 0.002959 ± 0.000022 and 0.1020 ± 0.0008, respectively (Eberhardt et al. 1965). Honda et al. (2015) recently re-determined atmospheric Ne isotope composition, in particular revising ^{21}Ne/^{20}Ne to be 0.002905 ± 0.000003.

Atmospheric neon is ubiquitous in mineral samples, even those that have crystallized deep in Earth with no contact with air. It is likely that much of the air-derived Ne in minerals is absorbed onto mineral surfaces. However, extremely high concentrations are measured in quartz, often probably in fluid inclusions (Graf et al. 1991; Niedermann et al. 1993). The mixture of atmospheric and cosmogenic neon in samples always lies on the "spallation line" in Fig. 1.

4.2 Nucleogenic Ne

Neon isotopes are produced by an array of nuclear reactions in minerals. The dominant source of nucleogenic Ne is by (α, n) reactions with ^{18}O (^{21}Ne) and ^{19}F (^{22}Ne), and (n, α) reactions with ^{24}Mg (^{21}Ne) and ^{25}Mg (^{22}Ne) (Graf et al. 1991; Niedermann et al. 1993). The α-particles are generated by radioactive decay of U and Th or spontaneous fission of ^{238}U. Thermal neutrons are generated during (α, n) reactions, and by cosmic ray spallation, termed cosmic ray thermal neutrons (CTN) (Dunai et al. 2007). The effect of these reactions is shown in Fig. 1.

The concentration of target elements F and Mg are negligible in quartz, so the dominant nucleogenic Ne production is ^{18}O(α, n)^{21}Ne. Addition of this mono-isotopic component tends to produce data that plot to the right of the air-spallation line in the neon three-isotope diagram (Fig. 1). U and Th concentrations are typically low in pure quartz, but are often located in accessory mineral inclusions, e.g., biotite, apatite, and zircon (Schäfer et al. 2002). α-particles recoil 10–40 μm during production, and can be implanted into the outer few 10's μm of grains. As nucleogenic Ne is located in the crystal lattice of quartz, it is released with cosmogenic neon predominantly below 800 °C. The removal of the rims of quartz grains by acid etching can reduce the nucleogenic component (Kohl and Nishiizumi 1992). On the other hand, analysis of shielded samples with the exposed lithology can be used to quantify the contribution of non-cosmogenic nuclides (e.g., Margerison et al. 2005).

Crustal fluids are typically enriched in nucleogenic ^{21}Ne and ^{22}Ne, acquired by water–rock interaction during fluid circulation in the crust (Kennedy et al. 1990). When these fluids are trapped as inclusions in minerals they impart nucleogenic Ne. The isotopic composition of the fluid depends on the O/F ratio of the crust (Ballentine and Burnard 2002; Kennedy et al. 1990). Kennedy et al. (1990) have shown that crustal fluids typically have higher ^{22}Ne/^{21}Ne ratios than that of cosmogenic Ne (Fig. 1), but it may not always be possible to distinguish cosmogenic neon. Usually the inclusion-hosted volatiles require higher release temperatures than cosmogenic Ne during stepwise heating experiments and it may be possible to separate the two components and allow cosmogenic Ne to be quantified (Niedermann et al. 1994).

4.3 Mantle Ne

Mantle-derived neon is enriched in ^{20}Ne and ^{21}Ne relative to air Ne. It is typically incorporated in magmatic minerals at the time of rock formation, and usually dominantly presents as melt or vapor inclusions. It should be clearly identified because of its distinct isotopic composition, whose trend is almost perpendicular to the spallation line (Fig. 1).

4.4 Inherited cosmogenic Ne

Cosmogenic Ne that has been produced prior to the exposure event that brought rocks to the surface will not, in contrast to the radionuclides, decay away. It will be isotopically indistinguishable from modern cosmogenic Ne

and, if not identified, will exaggerate exposure durations and lower erosion rates. While it is widely recognized in attempts to date the deposition of modern sediments (e.g., Ma et al. 2016), it is also likely to be a problem in the analysis of bedrock and boulders made of sedimentary or meta-sedimentary rocks which may be composed of detrital quartz that was exposed during erosion and transport of the grains that made up the sediment prior to lithification.

There are several approaches to determining the amount of cosmogenic Ne in a mineral. The most common is to quantify and remove the atmospheric ^{21}Ne:

$$^{21}\mathrm{Ne}_{\mathrm{ex}} = {}^{20}\mathrm{Ne}_{\mathrm{mea}} \times \left[\left(^{21}\mathrm{Ne}/^{20}\mathrm{Ne}\right)_{\mathrm{mea}} - \left(^{21}\mathrm{Ne}/^{20}\mathrm{Ne}\right)_{\mathrm{air}}\right] \quad (6)$$

where, $^{21}\mathrm{Ne}_{\mathrm{ex}}$ is typically a mixture of in-situ and crustal nucleogenic Ne, and cosmogenic Ne. The non-cosmogenic (mantle and nucleogenic) component of the excess ^{21}Ne can be measured in deeply shielded samples of the same lithology as analyzed for cosmogenic Ne. In modern sedimentary deposits the cosmogenic Ne generated during erosion and transport can be determined using the depth profile method (Anderson et al. 1996; Hetzel et al. 2002a). If no post-depositional displacement of the deposit occurred, and the transport and depositional processes were invariant in the sedimentary sequence, the concentration of cosmogenic Ne should decrease exponentially with depth, and a concentration versus depth plot should asymptotically approach the mean inheritance at depths of greater than 2 m (Fig. 3) (e.g., Ma et al. 2016). Other approaches to correcting for nucleogenic Ne concentrations include calculating the in-situ contribution from measured radioelement concentrations and the algorithm of Yatsevich and Honda (1997), and using the measured radiogenic ^{40}Ar and/or fissiogenic Xe isotopes to quantify the amount of trapped crustal ^{21}Ne (e.g., Fujioka et al. 2005).

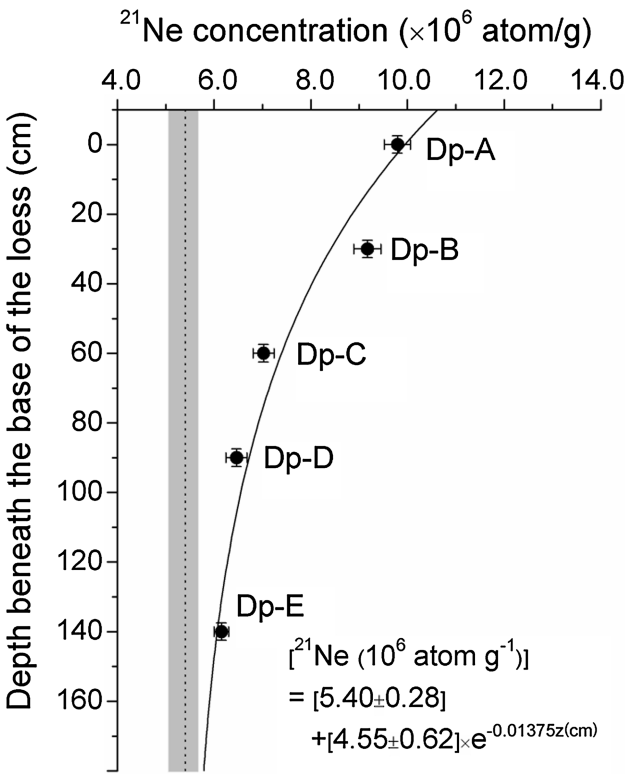

Fig. 3 The cosmogenic ^{21}Ne concentration profile, showing the amount of ^{21}Ne inheritance in terrace deposits (Ma et al. 2016). *Error bars* represent 1σ uncertainties. The *black curve* is the fitted exponential function. The *dashed line* and the margins of the *light gray band* correspond to the value of ^{21}Ne inheritance and its error boundaries

5 Applications of cosmogenic Ne

5.1 Exposure age determinations under independent constraint on erosion rate

The presence of non-cosmogenic neon components in minerals adds uncertainty to the accuracy of exposure age determined by cosmogenic ^{21}Ne. Nevertheless, cosmogenic ^{21}Ne is produced and retained in a range of minerals and thus has the potential for constraining the timing of the exposure of surfaces that cannot be studied with ^{10}Be, ^{26}Al, or ^{36}Cl.

Cosmogenic ^{3}He, in olivine and pyroxene phenocrysts, has been widely applied for dating the eruption of Pleistocene and Holocene basalt lavas where ^{14}C-datable material is not present (e.g., Foeken et al. 2009; Kurz 1986). Helium isotope determinations are easier than neon isotopes, and uncertainties associated with ^{3}He-derived exposure ages are typically lower than those of cosmogenic ^{21}Ne. In several studies, cosmogenic ^{21}Ne has been measured on the same samples in order to confirm the ^{3}He-derived exposure ages (Espanon et al. 2014; Fenton and Niedermann 2014; Gillen et al. 2010; Sarda et al. 1993; Staudacher and Allègre 1993). However, helium has only two isotopes, and thus the correction for non-cosmogenic components is complex. The three Ne isotopes allow a more effective resolution of the contribution from the cosmogenic component (e.g., Staudacher and Allègre 1993), but it is still difficult to detect small amounts of cosmogenic ^{21}Ne in the presence of relatively large amounts of non-cosmogenic ^{21}Ne.

As well as dating the eruption age of basalts, cosmogenic noble gas isotopes can be used to determine the time that basalts were eroded. Cerling et al. (1994) determined the timing of flood events by measuring the cosmogenic ^{3}He and ^{21}Ne exposure ages of eroded basalt boulders and scoured bedrock of the Big Lost River on the Snake River Plain, Colorado, USA. However, they noted that flood

surface samples had a range of cosmogenic ^{3}He and ^{21}Ne concentrations. A small number of the surface samples appear to have slightly higher concentrations, consistent with the inheritance of cosmogenic nuclides that were produced prior to the exposure of new surface during flooding.

Cosmogenic radionuclides are commonly used to study glacial histories (e.g., Ivy-Ochs et al. 1995). Cosmogenic ^{21}Ne has been less commonly exploited in the study of glacial landforms but holds huge potential. Graf et al. (2007) used cosmogenic ^{10}Be and ^{21}Ne to date erratic boulders from the top of the Montoz anticline in the Jura Mountains, Switzerland, to establish the pre-last-glacial-maximum glacial history. Strasky et al. (2009b) used ^{10}Be and ^{21}Ne to show the continuous long-term exposure history of erratic boulders in southern Tibet, and investigated how sensitive the glacial system is to the North Atlantic climate forcing.

Cosmogenic ^{21}Ne has also been used to determine the time of sediment deposition, such as river terraces and alluvial fans. It is used in particular to confirm the simple exposure history of the sediment surface, ruling out periods of burial, and to correct for the cosmogenic ^{10}Be that is generated during erosion of bedrock and transport of clasts to the sedimentation site. Phillips et al. (1998) reported cosmogenic ^{21}Ne analysis of quartz sand derived from the Quaternary Bandelier Tuff to estimate the depositional ages of alluvium and soils on the alluvial plateau in New Mexico, USA. They employed a depth profile to constrain the concentration of inherited ^{21}Ne and determine inheritance- and burial-corrected ^{21}Ne exposure ages for individual surfaces of two terraces. Hetzel et al. (2002a) used ^{21}Ne to determine the exposure age of fluvial terraces, and demonstrated the importance of determining the trapped (non-cosmogenic) Ne components of samples. Cosmogenic Ne measured in boulders on ancient marine terraces from northern Spain has been used to determine tectonic history (Alvarez-Marrón et al. 2008). The long exposure history, 1–2 million years, includes periods of burial and suggests that a wave-cut platform was generated in the Pliocene, and then was uplifted in response to crustal deformation.

Codilean et al. (2008) tested the hypothesis that there is spatial variation in erosion in a river catchment by measuring cosmogenic Ne in 32 quartz pebbles in the Gaub River catchment, Namibia. This dataset was compared to predicted distribution using measured catchment-averaged erosion rates and mean slope values. The ^{21}Ne concentrations span nearly two orders of magnitude and are skewed to low values consistent with predicted patterns, which imply that the measured distribution is a signature of the spatial variation in erosion rates.

Later, Kober et al. (2009) employed ^{10}Be, ^{26}Al, and ^{21}Ne in river sand quartz from the Rio Lluta catchment in the arid area of northern Chile to determine catchment-wide denudation rates. Denudation rates derived from ^{21}Ne gave the lowest rates (12–17 m·Ma^{-1}). By comparing the catchment-wide ^{21}Ne-derived erosion rate with the headwater region erosion rates derived from ^{21}Ne/^{10}Be and ^{26}Al/^{10}Be nuclide pairs, the authors highlighted that ^{21}Ne can be used to determine the temporal variation in sediment transport processes.

Antón et al. (2012) used cosmogenic ^{10}Be and ^{21}Ne to understand the Cenozoic history of the Duero River in the Arribes Gorge. Exposure ages for surfaces at various levels in the incised Duero River suggest that the final 200–300 m of fluvial incision in the Arribes Gorge occurred at a rate of 2–3 mm/a over the last $\sim$100 ka.

The different half-lives of ^{10}Be and ^{26}Al have been exploited to determine duration of sediment burial, which can be used to determine sedimentation age and deposition rates (e.g., Balco and Stone 2005; Granger et al. 1997). Balco and Shuster (2009a) first reported the incorporation of ^{21}Ne into the burial dating method to date cave sediments from the Riverbluff Cave in Springfield and the sedimentation age of the Whippoorwill formation at the Pendleton clay pit near Pendleton, Missouri, USA. The authors established the feasibility of this method and showed the improved age range and accuracy of the ^{10}Be/^{21}Ne nuclide pair compared to that of ^{10}Be/^{26}Al. Subsequently, Davis et al. (2011) applied ^{10}Be, ^{26}Al, and ^{21}Ne to date the burial of the late Neogene sedimentary formations from central Jordan Valley, Israel. They obtained an age range of 3.5–5.3 Ma for Pliocene–early Pleistocene lacustrine sediments. This provided them with independent age constraints that were used in combination with magnetostratigraphy to understand the depositional history. Matmon et al. (2014) employed ^{21}Ne, ^{10}Be, and ^{26}Al to date the sedimentary sequences deposited in the Sedom Lagoon to investigate rift-forming and escarpment evolution along the Dead Sea fault, which reflects the Neogene development of the relative African-Arabian plate motion.

Low-relief bedrock surfaces typically occur at high altitude, and are commonly interpreted as remnants of paleo-surfaces that originally had a much larger extent (e.g., Clark et al. 2005). The bedrock peneplains can be used to infer a significant amount of rock uplift after their generation at low elevation. However, the duration such surfaces were preserved at high elevation and the rate at which they were modified by erosion are difficult to quantify. Strobl et al. (2012) combined ^{21}Ne and ^{10}Be data measured in quartz clasts to confirm the simple exposure history with low denudation rates (5–11 m·Ma^{-1}) of the peneplain in the north of Nam Co of the southern Tibetan Plateau, which indicates the stability of exposure history and landscape evolution in this area.

Cosmogenic nuclide dating provides not only the chronology of geological events, but also information about the rates of erosion and landscape evolution. Hetzel et al. (2002b) determined the long-term slip rate of active faults in Central Asia ($\sim$0.35 mm·a^{-1}) based on ^{21}Ne, ^{10}Be, and ^{26}Al exposure ages of the offset landforms. They noted that the rate is two orders of magnitude slower than earlier estimates based on assumed ages of the Last Glacial Maximum, indicating long-term preservation of geomorphic features in Central Asia. Goethals et al. (2009b) investigated the impact of faulting on erosion rates in low-relief landscape in the Bishop Tuff, using in-situ ^{21}Ne in quartz from an ignimbrite with a known eruption age of 760 $\pm$ 2 ka. Under the steady-state erosion assumption, they obtained a series of erosion rates of the sites with various fault activities, suggesting that tectonic activity does not affect erosion rates in a recognizable way in the low-relief landscape. Ma et al. (2016) employed ^{21}Ne to measure the long-term average surface erosion rate in the Shapotou area in the northern margin of the Tibetan Plateau. They confirmed steady-state erosion of cosmogenic ^{21}Ne in the sediment of this area by measuring ^{21}Ne concentrations in quartz collected from a series of river terraces. The same ^{21}Ne concentrations within measurement uncertainties in the highest two terraces only provided information about the erosion rate (0.54–0.72 cm·ka^{-1}) and not of the exposure duration of terraces.

Perhaps the most exciting potential for cosmogenic ^{21}Ne exposure dating is its application for understanding the surface history of other planets. The ability to remotely perform chemical analysis allows nuclide determination on planet surfaces, obviating the need for sample return missions. In the first study of this kind, Farley et al. (2014) used the Sample Analysis at Mars (SAM) instrument on the Curiosity rover to determine the concentrations of cosmogenic ^{3}He, ^{21}Ne, and ^{36}Ar in a mudstone from the floor of Gale Crater on Mars. They obtained consistent exposure ages from different isotopes with an average value of 78 $\pm$ 30 million years. Compared with the formation age (4.21 $\pm$ 0.35 billion years) of the rocks comprising the crater rim, which is constrained by K-Ar dating, the authors proposed a hypothesis of scarp retreat which caused the recent exposure of the mudstone after long-term burial from its deposition. The large uncertainty reflects the difficulty of making these measurements, and assumptions regarding the cosmic ray flux, but it shows a novel perspective for applications of cosmogenic noble gas isotopes in many new fields of Earth sciences and beyond in the near future.

5.2 Long-term landscape development in low erosion rate regions

The presence of air-derived Ne and nucleogenic ^{21,22}Ne in quartz means that cosmogenic Ne requires approximately 10 times the exposure required for ^{10}Be to obtain equivalent precision and accuracy. Most landscape elements from temperate climates that are theoretically datable with cosmogenic ^{21}Ne are prone to surface erosion. As a result, cosmogenic ^{21}Ne concentrations in landscape elements that are older than a few tens of thousands of years rarely reflect the timing of formation. Landscape elements from low erosion rate regions, e.g. where climate is arid and/or dry, can be preserved for millions of years, though on these timescales processes of burial and exhumation may complicate exposure histories. Cosmogenic ^{21}Ne is ideally suited for understanding the evolution history and stability of erosional and depositional landforms. Here we highlight two extensively studied regions: Antarctica and the High Andes of Peru and Chile.

Cosmogenic ^{21}Ne has proven a powerful tool for reconstructing the Plio-Pleistocene history of Antarctic glaciations, specifically understanding glacial volume fluctuations on both temporal and spatial scales, and addressing whether the Antarctic climate is decoupled from global climate variations or has been subject to similar fluctuations as took place elsewhere on the planet, i.e. the dynamic and stable glaciations variation hypothesis of climatic change in Antarctica. The extremely low erosion rates in the Dry Valleys allow cosmogenic nuclide exposure dating to be accurately applied over a much longer time range—up to millions of years. Several studies have focused on dating glacial advances and establishing the association of ancient glacial landforms with Antarctic climate changes (e.g., Bruno et al. 1997; Kong et al. 2010; Schäfer et al. 1999; Van der Wateren et al. 1999). Many of these studies have exploited pyroxene from Ferrar dolerite bedrock and boulders rather than quartz.

Exposure ages of $\sim$6.5 Ma for doleritic clasts from Sirius tillite at Mount Fleming constrained the uplift rates of the Transantarctic Mountain to less than 170 m·Ma^{-1} (Bruno et al. 1997). Extraordinarily high surface exposure ages of 10 Ma for a dolerite boulder from Mount Fleming obtained by Schäfer et al. (1999) and 11.2 Ma for a bedrock sample from Daniels Range obtained by Van der Wateren et al. (1999) support the hypothesis of a stable East Antarctic Ice Sheet since at least late Miocene time and imply the decoupled climate variations of Antarctica from lower southern latitude regions.

Summerfield et al. (1999) first focused on measuring surface process rates of this extremely old landscape, and they estimated the long-term denudation rate in the Dry Valleys area of the Transantarctic Mountains, southern Victoria Land from the concentrations of cosmogenic ^{21}Ne measured in quartz in both sandstones and granitic basement. The denudation rates were proven sensitive to the landform elements, ranging from 0.26 to 1.02 m·Ma^{-1} for the rectilinear slopes down to 0.133–0.164 m·Ma^{-1} for the high-elevation surface sites. Oberholzer et al. (2003) combined ^{21}Ne with ^{3}He and ^{10}Be to age-limit Plio-

Pleistocene glaciations in the Deep Freeze Range in northern Victoria Land. They measured surface exposure ages and erosion rates of both the bedrock and glacial erratic, and using an erosion rate of 20 cm·Ma^{-1}, they obtained a mid-Pliocene exposure age of the landscape surface in the McMurdo Dry Valleys, which indicates a constantly cold and hyperarid climate in this area. Surface cobbles on moraines in the Vemier Valley, located at the inland edge of the Dry Valleys region were analyzed to provide age control of the glacier activity by Staiger et al. (2006). They used a conservative erosion rate of 5 cm·Ma^{-1} in age calculations, and obtained a series of cosmogenic ^{21}Ne exposure ages of old moraines of Ferrar dolerite. Subsequently, they used a modern moraine cobble sample to constrain the inheritance component in old moraines, and the cosmogenic age for the modern moraine suggested a value for nuclide inheritance of about 50 ka, which was less than 5% of the total exposure time of the oldest boulders.

To address the response of Antarctic ice sheets to global climate changes, Oberholzer et al. (2008) measured ^{21}Ne concentrations in rock surfaces of nunataks in northern Victoria Land to investigate the duration of exposure generated. They gave the first absolute ages of 3.5 Ma, which recorded the ice-free duration in this area. Strasky et al. (2009a) determined the exposure ages of the erratic boulders taking surface erosion into account, and the dating results mirrored the low-amplitude Pleistocene variations in the East Antarctic Ice Sheet, Victoria Land. Kong et al. (2010) applied the multiple nuclides ^{21}Ne–^{10}Be–^{26}Al to fit the surface exposure age of the bedrock on Mount Harding to $\sim$6.3 Ma, which recorded the time the East Antarctic Ice Sheet retreated below the summit of Mount Harding and suggested the important impact of moisture transport from the Southern Ocean on the ice sheet expansion in the interior of East Antarctica. Altmaier et al. (2010) reported a series of rock exposure ages for the Queen Maud Land, Antarctica. They used ^{21}Ne to date the samples in which radionuclide concentrations had nearly been saturated, and obtained minimum ^{21}Ne exposure ages longer than 8 Ma, which preculdes the presence of warm and humid climatic conditions during this period. Recently, Hein et al. (2016) presented geomorphological evidence and multiple cosmogenic nuclide data from the southern Ellsworth Mountains to suggest that the divide of the West Antarctic Ice Sheet has fluctuated only modestly in location and thickness for at least the last 1.4 million years.

The western central Andes are tectonically active and in-situ cosmogenic nuclides allow the relationship between erosion, tectonics, and climate on landscape evolution to be determined. The Atacama Desert is the driest place on Earth, and the onset of the aridification of the Atacama has been reported to be at least late Miocene (Dunai et al. 2005), as indicated by the ^{21}Ne ages of individual clasts on depositional surfaces ranging from 9 to 37 Ma. To investigate whether the slow landscape evolution is characteristic of the entire Atacama, or only of specific regions or landscape elements, Placzek et al. (2010) employed ^{10}Be, ^{26}Al, and ^{21}Ne to quantify the exposure history of a wide variety of landscape elements—including bedrock, alluvial fans, stream sediment, and boulders—along a transect across the Central Atacama. Their dating results as well as the field observations indicate the Central Atacama is more active than the Northern Atacama, and has remained geomorphically active well into the Pleistocene.

5.3 Perspective

In the past few decades, in-situ produced cosmogenic ^{21}Ne has found a broad range of applications in many fields of Earth surface process studies. Most of these studies have utilized quartz. However, the retention of cosmogenic ^{21}Ne in most other silicate and oxide minerals will no doubt open new areas of surface process research.

Developments in the ability to precisely measure smaller amounts of Ne will continue. Newly developed amplifiers with 10^{12} and 10^{13} Ω feedback resistors with fast response times and low noise characteristics offer the possibility of more stable measurement of small ion beam currents, and improved measurement precision. Combined Faraday-electron multiplier detectors will provide flexibility in analysis protocols. Increased resolution of new generation noble gas mass spectrometers is starting to provide separation of isobaric interferences and thus more accurate and precise measurement. This has, so far, extended as far as separation of ^{20}Ne^{+} and ^{40}Ar^{2+}. Laser heating systems minimize the noble gas blanks and hence will lower detection limits, and allow precise and accurate measurements from smaller samples.

Acknowledgements This work was supported by the basic scientific research fund, Institute of Geology, China Earthquake Administration (Grant Nos. IGCEA1504 and IGCEA1417), and the authors express their thanks for China Scholarship Council (CSC) who have sponsored the first author's visit in Scottish Universities Environmental Research Centre.

Compliance with ethical standards

Conflict of interest The authors declare that they have no conflict of interests.

References

Altmaier M, Herpers U, Delisle G, Merchel S, Ott U (2010) Glaciation history of Queen Maud Land (Antarctica) reconstructed from *in-situ* produced cosmogenic ^{10}Be, ^{26}Al and ^{21}Ne. Polar Sci 4:42–61

Alvarez-Marrón J, Hetzel R, Niedermann S, Menéndez R, Marquínez J (2008) Origin, structure and exposure history of a wave-cut platform more than 1 Ma in age at the coast of northern Spain: a multiple cosmogenic nuclide approach. Geomorphology 93:316–334

Anderson RS, Repka JL, Dick GS (1996) Explicit treatment of inheritance in dating depositional surfaces using *in-situ* ^{10}Be and ^{26}Al. Geology 24:47–51

Antón L et al (2012) Quantification of fluvial incision in the Duero Basin (NW Iberia) from longitudinal profile analysis and terrestrial cosmogenic nuclide concentrations. Geomorphology 165:50–61

Balco G, Shuster DL (2009a) ^{26}Al–^{10}Be–^{21}Ne burial dating. Earth Planet Sci Lett 286:570–575

Balco G, Shuster DL (2009b) Production rate of cosmogenic ^{21}Ne in quartz estimated from ^{10}Be, ^{26}Al, and ^{21}Ne concentrations in slowly eroding Antarctic bedrock surfaces. Earth Planet Sci Lett 281:48–58

Balco G, Stone JO (2005) Measuring middle Pleistocene erosion rates with cosmic-ray-produced nuclides in buried alluvial sediment, Fisher Valley, southeastern Utah. Earth Surf Process Landf 30:1051–1067

Balco G, Stone JO, Lifton NA, Dunai TJ (2008) A complete and easily accessible means of calculating surface exposure ages or erosion rates from ^{10}Be and ^{26}Al measurements. Quat Geochronol 3:174–195

Ballentine CJ, Burnard PG (2002) Production, release and transport of noble gases in the continental crust. Rev Mineral Geochem 47:481–538

Barbouti A, Rastin B (1983) A study of the absolute intensity of muons at sea level and under various thicknesses of absorber. J Phys G: Nucl Phys 9:1577–1595

Benedetti L et al (2002) Post-glacial slip history of the Sparta fault (Greece) determined by ^{36}Cl cosmogenic dating: evidence for non-periodic earthquakes. Geophys Res Lett. doi:10.1029/2001GL014510

Borchers B et al (2016) Geological calibration of spallation production rates in the CRONUS-Earth project. Quat Geochronol 31:188–198

Braucher R, Merchel S, Borgomano J, Bourlès D (2011) Production of cosmogenic radionuclides at great depth: a multi element approach. Earth Planet Sci Lett 309:1–9

Brown ET, Bourlès D, Colin F, Raisbeck GM, Yiou F, Desgarceaux S (1995) Evidence for muon-induced production of ^{10}Be in near-surface rocks from the Congo. Geophys Res Lett 22:703–706

Bruno LA, Baur H, Graf T, Schlu C, Signer P, Wieler R (1997) Dating of Sirius group tillites in the Antarctic Dry Valleys with cosmogenic ^{3}He and ^{21}Ne. Earth Planet Sci Lett 147:37–54

Cerling TE, Poreda RJ, Rathburn SL (1994) Cosmogenic ^{3}He and ^{21}Ne age of the big lost river flood, Snake River plain, Idaho. Geology 22:227–230

Clark DH, Bierman PR, Larsen P (1995) Improving *in-situ* cosmogenic chronometers. Quat Res 44:367–377

Clark MK, House M, Royden L, Whipple K, Burchfiel B, Zhang X, Tang W (2005) Late Cenozoic uplift of southeastern Tibet. Geology 33:525–528

Codilean AT, Bishop P, Stuart FM, Hoey TB, Fabel D, Freeman SP (2008) Single-grain cosmogenic ^{21}Ne concentrations in fluvial sediments reveal spatially variable erosion rates. Geology 36:159–162

Davis M, Matmon A, Fink D, Ron H, Niedermann S (2011) Dating Pliocene lacustrine sediments in the central Jordan Valley, Israel—implications for cosmogenic burial dating. Earth Planet Sci Lett 305:317–327

Desilets D, Zreda M (2003) Spatial and temporal distribution of secondary cosmic-ray nucleon intensities and applications to *in-situ* cosmogenic dating. Earth Planet Sci Lett 206:21–42

Desilets D, Zreda M, Prabu T (2006) Extended scaling factors for *in-situ* cosmogenic nuclides: new measurements at low latitude. Earth Planet Sci Lett 246:265–276

Dunai T (2001) Influence of secular variation of the geomagnetic field on production rates of *in-situ* produced cosmogenic nuclides. Earth Planet Sci Lett 193:197–212

Dunai TJ, López GAG, Juez-Larré J (2005) Oligocene–Miocene age of aridity in the Atacama Desert revealed by exposure dating of erosion-sensitive landforms. Geology 33:321–324

Dunai TJ, Stuart FM, Pik R, Burnard P, Gayer E (2007) Production of ^{3}He in crustal rocks by cosmogenic thermal neutrons. Earth Planet Sci Lett 258:228–236

Eberhardt P, Eugster O, Marti K (1965) Notizen: a redetermination of the isotopic composition of atmospheric neon. Z Naturforsch A 20:623–624

Espanon VR, Honda M, Chivas AR (2014) Cosmogenic ^{3}He and ^{21}Ne surface exposure dating of young basalts from Southern Mendoza, Argentina. Quat Geochronol 19:76–86

Evenstar LA, Stuart FM, Hartley AJ, Tattitch B (2015) Slow Cenozoic uplift of the western Andean Cordillera indicated by cosmogenic ^{3}He in alluvial boulders from the Pacific Planation Surface. Geophys Res Lett 42:8448–8455

Farley K et al (2014) *In-situ* radiometric and exposure age dating of the Martian surface. Science 343:1247166

Fenton CR, Niedermann S (2014) Surface exposure dating of young basalts (1–200 ka) in the San Francisco volcanic field (Arizona, USA) using cosmogenic ^{3}He and ^{21}Ne. Quat Geochronol 19:87–105

Foeken JP, Day S, Stuart FM (2009) Cosmogenic ^{3}He exposure dating of the Quaternary basalts from Fogo, Cape Verdes: implications for rift zone and magmatic reorganisation. Quat Geochronol 4:37–49

Foeken JP, Stuart FM, Mark DF (2012) Long-term low latitude cosmogenic ^{3}He production rate determined from a 126 ka basalt from Fogo, Cape Verdes. Earth Planet Sci Lett 359:14–25

Fujioka T, Chappell J, Honda M, Yatsevich I, Fifield K, Fabel D (2005) Global cooling initiated stony deserts in central Australia 2–4 Ma, dated by cosmogenic ^{21}Ne–^{10}Be. Geology 33:993–996

Gillen D, Honda M, Chivas AR, Yatsevich I, Patterson D, Carr PF (2010) Cosmogenic ^{21}Ne exposure dating of young basaltic lava flows from the Newer Volcanic Province, western Victoria, Australia. Quat Geochronol 5:1–9

Goehring BM, Kurz MD, Balco G, Schaefer JM, Licciardi J, Lifton N (2010) A reevaluation of *in-situ* cosmogenic ^{3}He production rates. Quat Geochronol 5:410–418

Goethals M et al (2009a) An improved experimental determination of cosmogenic ^{10}Be/^{21}Ne and ^{26}Al/^{21}Ne production ratios in quartz. Earth Planet Sci Lett 284:187–198

Goethals M, Niedermann S, Hetzel R, Fenton C (2009b) Determining the impact of faulting on the rate of erosion in a low-relief landscape: a case study using *in-situ* produced ^{21}Ne on active normal faults in the Bishop Tuff, California. Geomorphology 103:401–413

Gosse JC, Phillips FM (2001) Terrestrial *in-situ* cosmogenic nuclides: theory and application. Quat Sci Rev 20:1475–1560

Graf T, Kohl C, Marti K, Nishiizumi K (1991) Cosmic-ray produced neon in Antarctic rocks. Geophys Res Lett 18:203–206

Graf AA, Strasky S, Ivy-Ochs S, Akçar N, Kubik PW, Burkhard M, Schlüchter C (2007) First results of cosmogenic dated pre-Last Glaciation erratics from the Montoz area, Jura Mountains, Switzerland. Quat Int 164:43–52

Granger D, Riebe C (2007) Cosmogenic nuclides in weathering and erosion. Treatise Geochem 5:1–43

Granger DE, Smith AL (2000) Dating buried sediments using radioactive decay and muogenic production of ^{26}Al and ^{10}Be. Nucl Instrum Methods Phys Res B 172:822–826

Granger DE, Kirchner JW, Finkel RC (1997) Quaternary downcutting rate of the New River, Virginia, measured from differential decay of cosmogenic ^{26}Al and ^{10}Be in cave-deposited alluvium. Geology 25:107–110

Hein AS et al (2016) Evidence for the stability of the West Antarctic Ice Sheet divide for 1.4 million years. Nat Commun 7:10325

Hetzel R, Niedermann S, Ivy-Ochs S, Kubik PW, Tao M, Gao B (2002a) ^{21}Ne versus ^{10}Be and ^{26}Al exposure ages of fluvial terraces: the influence of crustal Ne in quartz. Earth Planet Sci Lett 201:575–591

Hetzel R, Niedermann S, Tao M, Kubik PW, Ivy-Ochs S, Gao B, Strecker MR (2002b) Low slip rates and long-term preservation of geomorphic features in Central Asia. Nature 417:428–432

Honda M, Zhang X, Phillips D, Hamilton D, Deerberg M, Schwieters JB (2015) Redetermination of the ^{21}Ne relative abundance of the atmosphere, using a high resolution, multi-collector noble gas mass spectrometer (HELIX-MC Plus). Int J Mass Spectrom 387:1–7

Ivy-Ochs S, Schlüchter C, Kubik PW, Dittrich-Hannen B, Beer J (1995) Minimum ^{10}Be exposure ages of early Pliocene for the Table Mountain plateau and the Sirius Group at Mount Fleming, Dry Valleys, Antarctica. Geology 23:1007–1010

Ivy-Ochs S et al (2006) The timing of glacier advances in the northern European Alps based on surface exposure dating with cosmogenic ^{10}Be, ^{26}Al, ^{36}Cl, and ^{21}Ne. Geol Soc Am Spec Pap 415:43–60

Kennedy B, Hiyagon H, Reynolds J (1990) Crustal neon: a striking uniformity. Earth Planet Sci Lett 98:277–286

Kober F, Ivy-Ochs S, Zeilinger G, Schlunegger F, Kubik P, Baur H, Wieler R (2009) Complex multiple cosmogenic nuclide concentration and histories in the arid Rio Lluta catchment, northern Chile. Earth Surf Process Landf 34:398–412

Kohl C, Nishiizumi K (1992) Chemical isolation of quartz for measurement of *in-situ*-produced cosmogenic nuclides. Geochim Cosmochim Acta 56:3583–3587

Kong P, Huang F, Liu X, Fink D, Ding L, Lai Q (2010) Late Miocene ice sheet elevation in the Grove Mountains, East Antarctica, inferred from cosmogenic ^{21}Ne–^{10}Be–^{26}Al. Glob Planet Change 72:50–54

Kurz MD (1986) *In-situ* production of terrestrial cosmogenic helium and some applications to geochronology. Geochim Cosmochim Acta 50:2855–2862

Lal D (1991) Cosmic ray labeling of erosion surfaces: *in-situ* nuclide production rates and erosion models. Earth Planet Sci Lett 104:424–439

Lal D, Peters B (1967) Cosmic ray produced radioactivity on the earth. In: Sitte K (ed) Cosmic rays. Springer, Berlin, pp 551–612

Lifton NA, Bieber JW, Clem JM, Duldig ML, Evenson P, Humble JE, Pyle R (2005) Addressing solar modulation and long-term uncertainties in scaling secondary cosmic rays for *in-situ* cosmogenic nuclide applications. Earth Planet Sci Lett 239:140–161

Lifton N, Sato T, Dunai TJ (2014) Scaling *in-situ* cosmogenic nuclide production rates using analytical approximations to atmospheric cosmic-ray fluxes. Earth Planet Sci Lett 386:149–160

Ma Y, Wu Y, Li D, Zheng D (2015) Analytical procedure of neon measurements on GV 5400 noble gas mass spectrometer and its evaluation by quartz standard CREU-1. Int J Mass Spectrom 380:26–33

Ma Y et al (2016) Erosion rate in the Shapotou area, northwestern China, constrained by *in-situ*-produced cosmogenic ^{21}Ne in long-exposed erosional surfaces. Quat Geochronol 31:3–11

Margerison H, Phillips W, Stuart F, Sugden D (2005) An assessment of cosmogenic ^{3}He surface exposure dating in the Northern Dry Valleys of East Antarctica. Earth Planet Sci Lett 230:163–175

Marrero SM, Phillips FM, Borchers B, Lifton N, Aumer R, Balco G (2016) Cosmogenic nuclide systematics and the CRONUScalc program. Quat Geochronol 31:160–187

Masarik J, Reedy RC (1995) Terrestrial cosmogenic-nuclide production systematics calculated from numerical simulations. Earth Planet Sci Lett 136:381–395

Matmon A, Fink D, Davis M, Niedermann S, Rood D, Frumkin A (2014) Unraveling rift margin evolution and escarpment development ages along the Dead Sea fault using cosmogenic burial ages. Quat Res 82:281–295

Niedermann S (2000) The ^{21}Ne production rate in quartz revisited. Earth Planet Sci Lett 183:361–364

Niedermann S (2002) Cosmic-ray-produced noble gases in terrestrial rocks: dating tools for surface processes. Rev Mineral Geochem 47:731–784

Niedermann S, Graf T, Marti K (1993) Mass spectrometric identification of cosmic-ray-produced neon in terrestrial rocks with multiple neon components. Earth Planet Sci Lett 118:65–73

Niedermann S, Graf T, Kim J, Kohl C, Marti K, Nishiizumi K (1994) Cosmic-ray-produced ^{21}Ne in terrestrial quartz: the neon inventory of Sierra Nevada quartz separates. Earth Planet Sci Lett 125:341–355

Nishiizumi K, Winterer E, Kohl C, Klein J, Middleton R, Lal D, Arnold J (1989) Cosmic ray production rates of ^{10}Be and ^{26}Al in quartz from glacially polished rocks. J Geophys Res Solid Earth 94:17907–17915

Oberholzer P et al (2003) Limited pliocene/pleistocene glaciation in Deep Freeze Range, northern Victoria Land, Antarctica, derived from *in-situ* cosmogenic nuclides. Antarct Sci 15:493–502

Oberholzer P, Baroni C, Salvatore M, Baur H, Wieler R (2008) Dating late Cenozoic erosional surfaces in Victoria Land, Antarctica, with cosmogenic neon in pyroxenes. Antarct Sci 20:89–98

Phillips WM, McDonald EV, Reneau SL, Poths J (1998) Dating soils and alluvium with cosmogenic ^{21}Ne depth profiles: case studies from the Pajarito Plateau, New Mexico, USA. Earth Planet Sci Lett 160:209–223

Phillips FM et al (2016) The CRONUS-earth project: a synthesis. Quat Geochronol 31:119–154

Placzek C, Matmon A, Granger D, Quade J, Niedermann S (2010) Evidence for active landscape evolution in the hyperarid Atacama from multiple terrestrial cosmogenic nuclides. Earth Planet Sci Lett 295:12–20

Portenga EW, Bierman PR (2011) Understanding Earth's eroding surface with ^{10}Be. GSA Today 21:4–10

Sarda P, Staudacher T, Allègre CJ, Lecomte A (1993) Cosmogenic neon and helium at Réunion: measurement of erosion rate. Earth Planet Sci Lett 119:405–417

Schäfer JM, Ivy-Ochs S, Wieler R, Leya I, Baur H, Denton GH, Schlüchter C (1999) Cosmogenic noble gas studies in the oldest landscape on earth: surface exposure ages of the Dry Valleys, Antarctica. Earth Planet Sci Lett 167:215–226

Schäfer JM et al (2002) The limited influence of glaciations in Tibet on global climate over the past 170 000 yr. Earth Planet Sci Lett 194:287–297

Shuster DL, Farley KA (2005) ^{4}He/^{3}He thermochronometry: theory, practice, and potential complications. Rev Mineral Geochem 58:181–203

Staiger J, Marchant D, Schaefer J, Oberholzer P, Johnson J, Lewis A, Swanger K (2006) Plio-pleistocene history of Ferrar Glacier, Antarctica: implications for climate and ice sheet stability. Earth Planet Sci Lett 243:489–503

Staudacher T, Allègre CJ (1993) Ages of the second caldera of Piton de la Fournaise volcano (Réunion) determined by cosmic ray produced ^{3}He and ^{21}Ne. Earth Planet Sci Lett 119:395–404

Stone J, Vasconcelos P (2000) Studies of geomorphic rates and processes with cosmogenic isotopes—examples from Australia. J Conf Abs 5:961

Strasky S et al (2009a) Surface exposure ages imply multiple low-amplitude Pleistocene variations in East Antarctic ice sheet, Ricker Hills, Victoria Land. Antarct Sci 21:59–69

Strasky S, Graf AA, Zhao Z, Kubik PW, Baur H, Schlüchter C, Wieler R (2009b) Late Glacial ice advances in southeast Tibet. J Asian Earth Sci 34:458–465

Strobl M, Hetzel R, Niedermann S, Ding L, Zhang L (2012) Landscape evolution of a bedrock peneplain on the southern Tibetan Plateau revealed by *in-situ*-produced cosmogenic ^{10}Be and ^{21}Ne. Geomorphology 153:192–204

Summerfield M, Stuart F, Cockburn H, Sugden D, Denton G, Dunai T, Marchant D (1999) Long-term rates of denudation in the Dry Valleys, Transantarctic Mountains, southern Victoria Land, Antarctica based on *in-situ*-produced cosmogenic ^{21}Ne. Geomorphology 27:113–129

Van den Bogaard P, Schirnick C (1995) ^{40}Ar/^{39}Ar laser probe ages of Bishop Tuff quartz phenocrysts substantiate long-lived silicic magma chamber at Long Valley, United States. Geology 23:759–762

Van der Wateren FM, Dunai TJ, Van Balen RT, Klas W, Verbers AL, Passchier S, Herpers U (1999) Contrasting Neogene denudation histories of different structural regions in the Transantarctic Mountains rift flank constrained by cosmogenic isotope measurements. Glob Planet Change 23:145–172

Vermeesch P (2007) CosmoCalc: an Excel add-in for cosmogenic nuclide calculations. Geochem Geophys Geosyst. doi:10.1029/2006GC001530

Vermeesch P et al (2015) Interlaboratory comparison of cosmogenic ^{21}Ne in quartz. Quat Geochronol 26:20–28

Yatsevich I, Honda M (1997) Production of nucleogenic neon in the Earth from natural radioactive decay. J Geophys Res Solid Earth 102:10291–10298